ARTICLE

Biallelic loss-of-function variants in *ZNF142* are associated with a robust DNA methylation signature affecting a limited number of genomic loci

Mathis Hildonen[1,35], Andrea Ciolfi[2,35], Marco Ferilli[2,35], Camilla Cappelletti[2], Chadi Al Alam[3,4], David J. Amor[5], Tahsin Stefan Barakat[6,7], Valérie Benoit[8], Ohad Shmuel Birk[9], Bert Callewaert[10,11], Ana Cazurro-Gutiérrez[12,13], Matthias De Wachter[14], Martine Doco-Fenzy[15,16], Paulino Gómez-Puertas[17], Trine Bjørg Hammer[1,18], Rami Abou Jamra[19], Rauan Kaiyrzhanov[20], Shinichi Kameyama[21], Boris Keren[22], Christina Kresge[23], Ilona Krey[19], Damien Lederer[8], Iñigo Marcos-Alcalde[17], Reza Maroofian[20], Naomichi Matsumoto[21], Takeshi Mizuguchi[21], Lip-Hen Moey[24], Angela Morgan[25,26], Francina Munell[12,13], Konrad Platzer[19], Beth A. Pletcher[23], David Ros-Pardo[17], Lynne Rumping[27], Katalin Szakszon[28], Kristof Van Schil[27], Edgard Verdura[12], Julie Vogt[29], Evangeline Wassmer[30,31], Mina Zamani[32,33], Zeynep Tümer[1,34,36]✉ and Marco Tartaglia[2,36]✉

Biallelic inactivating variants in *ZNF142* underlie a clinically variable neurodevelopmental disorder. ZNF142 is a zinc-finger transcription factor with potential roles on chromatin organization, implying a possible association of ZNF142 loss of function with perturbed genome-wide DNA methylation (DNAm) pattern. We performed EPIC array-based methylation profiling of peripheral blood-derived DNA samples from 27 individuals with biallelic *ZNF142* inactivating variants, together with 6 heterozygous carriers and 40 controls. A DNAm signature discovery pipeline was applied by using 440 controls for discovery and validation analyses, and a machine-learning model was trained to classify 8 individuals carrying *ZNF142* variants of uncertain clinical significance. Analyses directed to explore the genome-wide DNAm landscape in affected individuals revealed 88 differentially methylated probes constituting the minimal informative set specific to ZNF142 loss of function. This reproducible pattern of DNAm changes involved regulatory regions of a small number of genes. The DNAm signature derived from peripheral blood allowed us to diagnose individuals carrying biallelic inactivating *ZNF142* variants when applied to fibroblasts. Our findings provide evidence that biallelic loss-of-function *ZNF142* variants result in a specific and robust DNAm signature. The identified DNAm pattern suggests occurrence of a methylation disturbance involving a small number of loci that appears to be shared by different cell lineages.

European Journal of Human Genetics (2025) 33:896–903; https://doi.org/10.1038/s41431-025-01876-z

[1]Department of Clinical Genetics, Copenhagen University Hospital, Rigshospitalet, 2100 Copenhagen, Denmark. [2]Molecular Genetics and Functional Genomics, Bambino Gesù Children's Hospital, IRCCS, 00146 Rome, Italy. [3]Department of Pediatric Neurology, American center for Psychiatry and Neurology, Abu Dhabi, UAE. [4]Department of Pediatric Neurology, Haykel Hospital, El Koura, Lebanon. [5]Department of Paediatrics, University of Melbourne, Murdoch Children's Research Institute, Melbourne, Australia. [6]Deparment of Clinical Genetics, Erasmus MC, 3000CA Rotterdam, The Netherlands. [7]ENCORE Expertise Center for Neurodevelopmental Disorders, Erasmus MC, University Medical Center, 3000CA Rotterdam, Netherlands. [8]IPG, Centre for Human Genetics, Charleroi, Belgium. [9]Genetics Institute, Soroka University Medical Center, Beer-Sheva, Israel. [10]Center for Medical Genetics, Ghent University Hospital, 9000 Ghent, Belgium. [11]Department of Biomolecular Medicine, Ghent University, 9000 Ghent, Belgium. [12]Paediatric Neurology Research Group, Vall d'Hebron Institut de Recerca, 08035 Barcelona, Spain. [13]Universitat Autònoma de Barcelona, 08193 Barcelona, Spain. [14]Department of Child Neurology, Antwerp University Hospital, University of Antwerp, Edegem, Belgium. [15]SFR CAP SANTE, Service de génétique CHU Reims, 51092 Reims, France. [16]CHU de Nantes, service de génétique médicale, 44000 Nantes, France. [17]Molecular Modeling Group, Centro de Biología Molecular Severo Ochoa, CBMSO (CSIC-UAM), E-28049 Madrid, Spain. [18]Department of Epilepsy Genetics and Personalized Treatment, Danish Epilepsy Centre, Dianalund, Denmark. [19]Institute of Human Genetics, University of Leipzig Medical Center Leipzig, 04103 Leipzig, Germany. [20]Department of Neuromuscular Disorders, University College London Institute of Neurology, WC1N 3BG London, UK. [21]Department of Human Genetics, Yokohama City University Graduate School of Medicine, 236-0004 Yokohama, Japan. [22]Department of Medical Genetics, Pitié-Salpêtrière Hospital, AP-HP.Sorbonne Université, 75013 Paris, France. [23]Rutgers New Jersey Medical School, Newark, NJ, USA. [24]Department of Clinical Genetics, Penang Hospital, 10450 Georgetown, Malaysia. [25]Speech and Language, Murdoch Children's Research Institute, 3052 Melbourne, Australia. [26]Department of Audiology and Speech Pathology, 3052 Melbourne, Australia. [27]Department of Medical Genetics, Antwerp University Hospital, University of Antwerp, 2650 Edegem, Belgium. [28]University of Debrecen, Faculty of Medicine, Clinical Center, Institute of Paediatrics, 4032 Debrecen, Hungary. [29]West Midlands Regional Genetics Service, Birmingham Women's and Children's Hospital, B15 2TG Birmingham, UK. [30]Neurology, Birmingham Women's and Children's Hospital, B4 6 NH Birmingham, UK. [31]Institute of Health and Neurodevelopment, Aston University, B4 7ET Birmingham, UK. [32]Center for Genomics and Systems Biology, Department of Biology, New York University, New York, NY 10003, USA. [33]Narges Medical Genetics and Prenatal Diagnosis Laboratory, Kianpars, Ahvaz, Iran. [34]Department of Clinical Medicine, Faculty of Medicine and Health Sciences, University of Copenhagen, 2100 Copenhagen, Denmark. [35]These authors contributed equally: Mathis Hildonen, Andrea Ciolfi, Marco Ferilli. [36]These authors jointly supervised this work: Zeynep Tümer, Marco Tartaglia. ✉email: Zeynep.tumer@regionh.dk; marco.tartaglia@opbg.net

Received: 4 March 2025 Revised: 23 April 2025 Accepted: 12 May 2025
Published online: 23 May 2025

INTRODUCTION

Homozygous or compound heterozygous loss-of-function (LoF) variants in the zinc-finger protein 142 gene (*ZNF142*; MIM *604083) underlie a syndromic neurodevelopmental disorder (NDD) with impaired speech and hyperkinetic movements, first described in 2019 (MIM #618425) [1]. To date, 43 affected individuals have been reported [1–9]. The disorder presents with clinical variability, and the major features include developmental delay (DD), intellectual disability (ID), behavioral anomalies, seizures, impaired motor function, and movement disorders [2].

ZNF142 encodes a member of the C2H2 zinc finger protein (ZFP) superfamily of transcription factors. The protein is characterized by two domains of tandemly arranged zinc finger (ZnF) motifs, which mediate DNA binding [10], and a Krüppel-associated box (KRAB) domain, which is involved in recruiting chromatin remodeling proteins (*e.g.*, KAP1/TRIM28) to DNA-binding sites [11, 12]. KRAB ZnF proteins (KRAB-ZFPs) regulate the expression of target genes by binding to their regulatory regions and recruiting cofactors, such as chromatin remodeling proteins [13], and contribute to various programs controlling brain development and function [12]. KRAB-ZFPs have been implicated in regulation of gene expression at transposable elements (TE) and imprinted regions by altering DNAm at selected loci [14–16]. The KRAB-ZFP/KAP1 system is supposed to serve as the first line of TE control upon chromatin decondensation occurring during early developmental stages, and KRAB-ZFP/KAP1-mediated silencing of TE has been shown to be required in some differentiated tissues, including neural lineages [17, 18].

Many rare genetic diseases are caused by variants in genes encoding proteins involved in epigenetic regulation, where mutations in single genes can affect the global epigenetic pattern of the cell [19]. For a number of these, disease-specific genome-wide patterns of DNAm (DNAm signatures or episignatures) have been identified [20]. These signatures can be investigated using peripheral blood derived DNA *via* DNAm arrays and are employed as a complementary diagnostic tool to assess whether the DNAm pattern of a patient matches the DNAm signature of a given disorder [20–23]. During the recent years, this approach has successfully been applied to speed up diagnosis of rare diseases, particularly to assess the pathogenicity of variants of uncertain significance (VUS), screen patients with uninformative molecular findings, and resolve clinical subtypes of a disorder [20, 24–26].

Given the role of KRAB-ZFPs in TE mediated chromatin remodeling, we investigated the presence of a genome-wide DNAm pattern specifically associated with biallelic inactivating *ZNF142* variants and identified a distinctive and robust DNAm signature for ZNF142 LoF in DNA from both peripheral blood cells and primary fibroblasts. Applying this signature, we were able to reclassify eight VUS, including two hypomorphic variants, likely partially explaining the clinical variability associated with biallelic pathogenic *ZNF142* variants.

MATERIALS AND METHODS

Study cohort

A total of 27 individuals with biallelic *ZNF142* variants were enrolled in the study (Table S1). Nineteen individuals (ID1 to ID19) had biallelic *ZNF142* variants classified as pathogenic (P) or likely pathogenic (LP) according to the American College of Medical Genetics (ACMG) criteria [27], eight individuals (ID20 to ID27) had either a P/LP variant and a VUS or two VUS, and six asymptomatic individuals (ID28 to ID33) were heterozygous for LP/P *ZNF142* variants (Table S2). Nineteen of these individuals had previously been reported [1, 2, 4, 9]. DNA specimens and clinical data from the subjects included in this study were collected, pseudonymized and stored in the context of routine diagnostic testing, following procedures in accordance with the ethical standards of the declaration of Helsinki protocols and subsequent versions after written signed informed consents from the participating individuals or parents/guardians were secured. The study was approved by the local institutional review board (Ethical Committee, Ospedale Pediatrico Bambino Gesù, ref. 1702_OPBG_2018, 2072_OPBG_2020 and PNRR-MR1-2022-12376811). The control group included 317 healthy individuals and 123 subjects with various molecularly confirmed disorders (Supplementary Methods).

Methylation analysis

Genomic DNA was extracted from peripheral blood (PB) or cultured skin fibroblasts (FBs) using standard protocols. DNA (500 ng) was bisulfite converted and hybridized to Illumina Infinium MethylationEPIC BeadChips (EPIC) v.1 (PB/FB) or v.2 (FB) arrays (Illumina, San Diego, CA, USA), which were scanned using the Illumina iScan platform. The 73 samples analyzed for this study were distributed across 16 different experimental batches to avoid bias.

For DNAm signature discovery and validation, DNAm profiling data analysis was performed according to a previously defined pipeline [28, 29]. Workflow and analytical steps are detailed in the Supplementary Methods.

A machine learning (ML) classification model based on the generated DNAm signature was used to classify the tested samples. The synthetic minority over-sampling technique (SMOTE) was applied to balance the ratio between patients and controls in the dataset prior to ML classifier training [30]. A support vector machine (SVM) model was tuned to find the best hyperparameters and accuracy by performing a five-fold cross-validation. After tuning, an SVM classifier was trained with a linear kernel using the *e1071* R package (v.1.7), using the "nu-classification" option [31]. SVM classifier scores (Platt's-scaled) below 0.3 were considered negative, between 0.3 and 0.5 were considered inconclusive, between 0.5 and 0.7 were considered supporting, while scores above 0.7 indicated a high-confidence occurrence of a match. To validate the ML classifier results, multidimensional scaling (MDS) plots and hierarchical clustering with heatmaps was calculated using the *ggplots2* package (v.3.4.2) [32], and inspected to ensure that patients and controls formed separate clusters. After validation, the DNAm signature was applied to test the samples from the individuals carrying *ZNF142* VUS and heterozygous carriers. Finally, the DNAm signature was applied to classify fibroblast cell line samples from two patients with biallelic *ZNF142* LoF variants, to assess the effectiveness of the DNAm in this tissue.

To investigate the possible functional relevance of ZNF142 LoF on the genome-wide DNAm pattern, the DMRcate package (v.2.12.0) was used to identify the differentially methylated regions (DMRs) in the 18 individuals carrying biallelic LoF ZNF142 variants [33]. By comparing affected individuals to healthy controls, regions containing at least five different CpGs within 1 kb with a minimum methylation difference of 5% and a false discovery rate (FDR) < 0.05 were extracted. Enrichment analysis for gene ontologies and pathways in the DMR data was performed using the missMethyl R package (v.1.32.1) [34]. To assess the concordance of DNAm changes between PB and FB tissues, the mean beta value change between affected individuals and controls in PB and FB was compared by linear regression on the most significant DMPs discovered in PB. Enrichment of DMRs for transposable elements was carried out using the GIGGLE score, which combines the estimation of the enrichment for observed versus expected (odds ratio), and Fisher's two tailed tests *p*-value [35], considering UCSC's RepeatMasker v.4.1.7 (http://www.repeatmasker.org).

Structural modeling of ZnF motifs and molecular dynamics simulation

Structural data analysis was carried out as previously reported [2]. Homology modeling of ZnF motifs 9–14 (encompassing Arg^{593}) and ZnF motifs 26–31 (encompassing Arg^{1500} and Val^{1553}), located respectively in the *N*-terminal and *C*-terminal ZnF clusters of human ZNF142 (UniprotKB ID: P52746) was performed using the crystal structure of ZnF motifs 5–8 of human CCCTC-binding factor in complex with DNA (PDB ID: 5K5I) [36], and of ZnF motifs 2–11 of mouse ZFP568 in complex with DNA (PDB ID: 5WJQ) [37] as templates. Gaps were modeled by combining predictions from Phyre 2 [38] and SwissModel [39]. Structure models were subjected to 200 ns of unrestrained molecular dynamics (MD) simulation using the Amber18 package (https://ambermd.org), essentially as previously described [40]. Trajectories were analyzed using CPPTRAJ [41] and VMD [42]. Figures were generated using the PyMOL Molecular Graphics System (https://pymol.org/2/).

RESULTS

DNAm signature identification and validation

Genome-wide DNAm profiling of DNA isolated from PB of 16 individuals with biallelic P/LP *ZNF142* variants (discovery cohort,

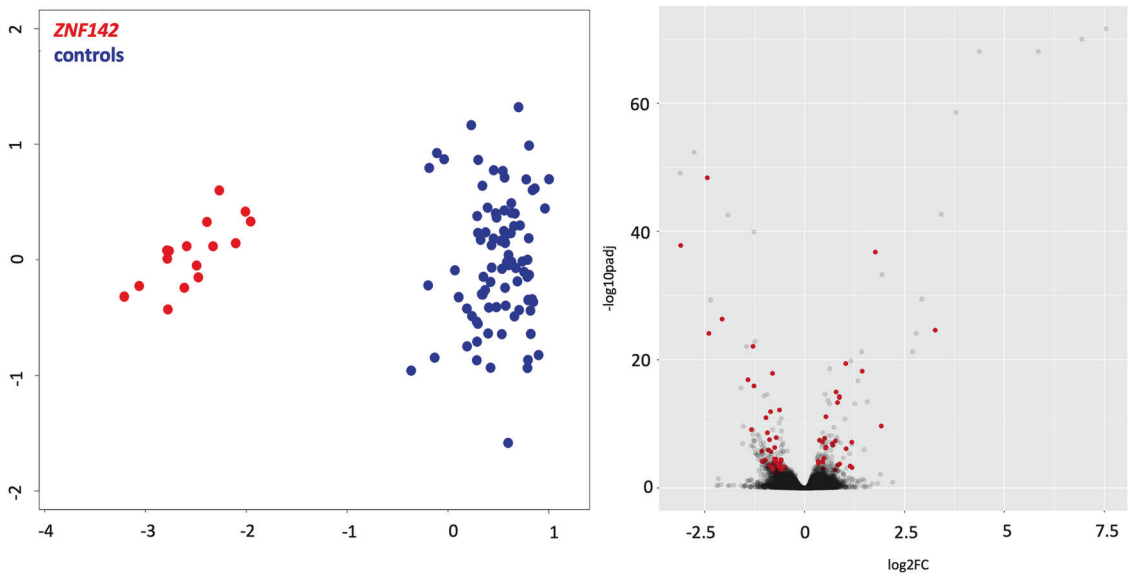

Fig. 1 Identification of a DNAm signature specific for the disorder caused by ZNF142 LoF. Clustering of the PB-derived DNA samples referring to the 16 affected individuals and 80 matched controls (discovery cohort) using the 88 probes defining the DNAm signature by multidimensional scaling (MDS) (left panel). All samples from individuals with biallelic *ZNF142* LoF variants (red dots) form a cluster separately from controls (blue dots). The Volcano plot illustrating the significance (−log10(padj)) and effect size (log2FC) of all CpGs from the linear model is also shown (right panel). Red dots denote the 88 selected probes included in the DNAm signature.

ID1 to ID16) was performed to test the occurrence of a specific DNAm signature associated with ZNF142 LoF. The age of the affected individuals ranged from 3 to 22 years at the time of sampling. Age, sex, and batch-matched control individuals ($N = 80$) comprised both healthy individuals ($N = 55$) and individuals affected by other rare disorders (RDs) ($N = 25$). Significant batch effects on the whole cohort were excluded by means of principal component analysis (PCA) (Fig. S1). Employing a three-tier strategy, a linear model was used to identify the most relevant DMPs in the discovery group, which was followed by a ROC analysis coupled to a final filtering step to remove the most correlated CpG sites (Pearson's > 0.90). The workflow was applied using first a leave-one-out cross-validation LOOV to each of the 16 samples from individuals with biallelic *ZNF142* LoF variants (Fig. S2), before employing the full discovery cohort to identify 88 probes constituting the minimal informative set defining the DNAm signature specific to the *ZNF142*-related disorder, characterized by an equal distribution of hyper- and hypomethylated sites (Fig. 1, Table S3). The selected probe set was applied on a second cohort (validation cohort) including two untested affected individuals carrying biallelic LoF *ZNF142* variants (ID17 and ID18) and 400 controls (277 apparently healthy individuals and 123 individuals affected with different RDs) (Fig. 2). All samples were correctly classified by both unsupervised (MDS and hierarchical clustering) and supervised (SVM classifier) analyses, the latter classifying all cases with high confidence (ID17 and ID18, SVM scores >0.90; controls, SVM sores <0.10). By testing the six asymptomatic individuals heterozygous for LP/P *ZNF142* variants (ID28 to ID33), who were parents of the enrolled affected individuals, we validated the sensitivity of the DNAm signature in properly discriminating gene dosage for LoF *ZNF142* variants (Fig. 2).

Finally, a new *limma* model using the previously identified top 500 DMPs was fitted comparing the heterozygous carriers with healthy controls to identify DNAm differences between the two groups. The 50 most significant DMPs from this analysis documented a clustering of the healthy carriers of *ZNF142* LoF variants, which could be separated from the healthy controls (Fig. S3).

Application of the DNAm signature in variant testing

The validated DNA probe set was subsequently used to classify eight individuals with inconclusive molecular findings ("testing cohort", ID20 to ID27; Tables S1 and S2). Two samples (ID20 and ID21) showed an intermediate position according to MDS analysis but were classified within the ZNF142 LoF group by hierarchical clustering. Consistently, the SVM-based classifier classified both samples as belonging to the *ZNF142* LoF group with relatively high confidence ($0.5 < \text{SVM scores} < 0.75$) (Fig. 2). The intermediate methylation status of the majority of the selected probes in these two samples, when compared to individuals with biallelic LoF *ZNF142* variants and controls, pointed to a likely hypomorphic behavior of the missense variants identified in these individuals (Fig. S4, Table S4). One of these individuals was compound heterozygous for two missense variants (p.Cys1233Phe and p.Arg1500Trp; ID20), while the second had a LoF and a missense variant (p.Arg636* and p.Phe1295Leu; ID21). The three amino acid changes were rare ($\text{MAF} < 2 \times 10^{-5}$) and predicted to affect protein function with high confidence by the AlphaMissense Pathogenicity tool (scores > 0.95) (Table S5). Consistently, previous structural analyses and molecular dynamics simulations supported disruptive consequences of these amino acid substitutions either by perturbing the overall structure of the individual ZnF motifs (p.Cys1233Phe and p.Phe1295Leu) or impairing DNA binding (p.Arg1500Trp), which was also mirrored by the relatively mild clinical phenotype of both individuals [2].

For the remaining six individuals (ID22 to ID27), the DNAm patterns were similar to controls in both unsupervised analyses and obtained SVM classifier scores < 0.10 (Fig. 2). Consistently, *a posteriori* segregation analysis in ID22 demonstrated that the two identified VUS (p.Gly1089Ser and p.Val780Ile) were both maternally inherited. Clinical reassessment of individuals ID23-ID26 from the same family and ID27 indicated that their clinical features did not fit (or only partially overlapped) with the phenotypic spectrum associated with biallelic LoF *ZNF142* variants. Specifically, ID23-ID26 showed spastic paraparesis with hyperreflexia and clonus in absence of DD/ID and seizures, while ID27's brain MRI documented occurrence of polymicrogyria, pachygyria, and subependymal heterotopias. Individuals ID23-ID26 were compound heterozygous

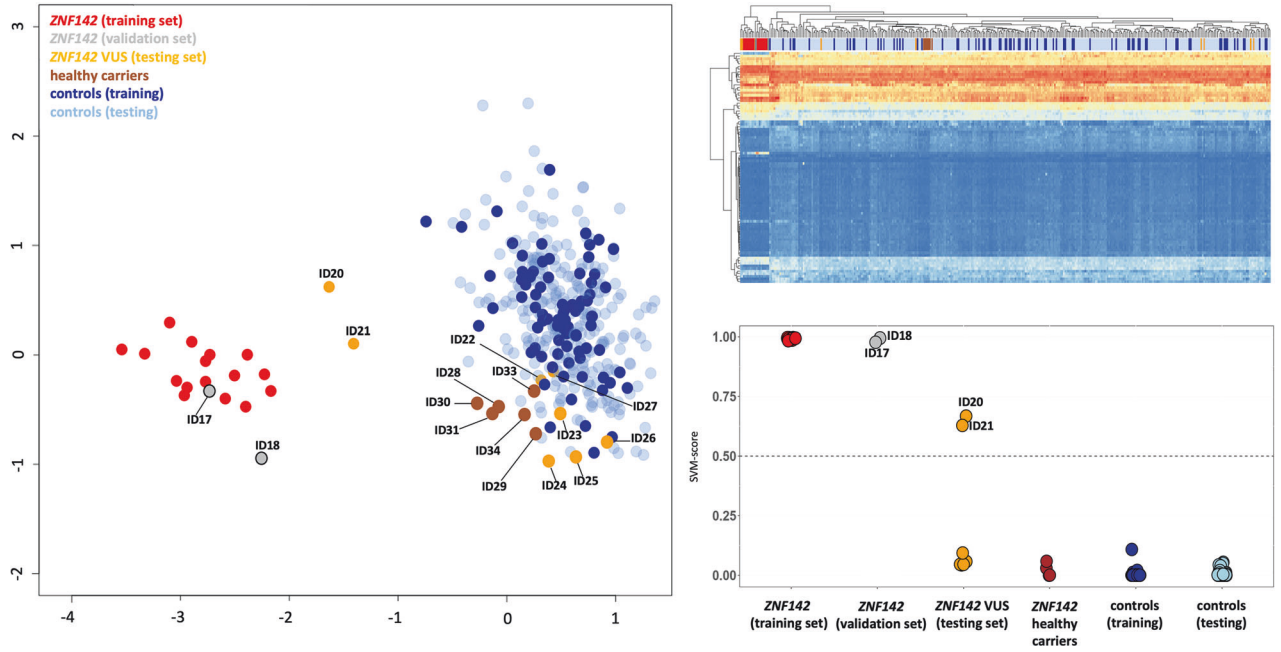

Fig. 2 The ZNF142 LoF-associated DNAm signature shows broad specificity and sensitivity. DNAm signature testing against a database containing hundreds of control individuals (healthy or affected by other NDDs) shows that all individuals with biallelic *ZNF142* LoF variants (discovery/training samples, red dots; validation samples, gray dots) cluster together by MDS (left panel) and unsupervised hierarchical clustering (right top panel) analyses. Six individuals with *ZNF142* VUS (orange dots) cluster with the controls (discovery and validation controls, dark and light blue dots, respectively), while two individuals with *ZNF142* VUS show an intermediate pattern. Individuals with heterozygous *ZNF142* LoF variants (maroon dots) cluster together with controls. Sample groups are indicated using color bars above the heatmap (red: fully methylated probes, blue: demethylated probes), using the same color code. The plot showing the prediction scores of the machine learning classifier (SVM) trained to recognize the DNAm signature of biallelic *ZNF142* LoF variants is also shown (right bottom panel). All discovery/training and validation samples carrying biallelic *ZNF142* LoF variants received scores close to 1, while all controls received scores close to 0. Among the eight individuals with *ZNF142* VUS variants, ID20 and ID21 received a score above 0.6, suggesting partial match with the DNAm signature, while the remaining six samples were tested negative.

for two rare/private missense variants (p.Gly1055Arg and p.Val1553Met), while ID27 was homozygous for a rare substitution, p.Arg593His. In line with the DNAm assessment, the AlphaMissense pathogenicity tool predicted a likely benign impact on protein function for these three amino acid substitutions (scores <0.50) (Table S5). Inspection of the possible structural consequences of the p.Gly1055Arg could not be carried out as Gly^{1055} is located in a large unstructured region (residues 596 to 1135) located between the two ZnF domains. Differently, the mutant ZnF motifs 9–14 modeled system showed a substantial rearrangement of the complex associated with the Arg-to-His substitution, suggesting loss of binding of the last ZnF motif to the DNA major groove, which was expected to impact proper ZNF142 interaction with DNA (Fig. S5). Thus far, no bona fide pathogenic missense change has been reported to affect any of the ZnF motifs located at the *N*-terminal ZnF cluster. Overall, these findings support the idea that the p.Arg593His does not share a hypomorphic behavior with the three missense changes affecting the *C*-terminal ZnF cluster.

Finally, we tested the robustness of the PB DNA-derived episignature to explore whether it could be successfully applied to variant classification using FB-derived DNA by testing two affected individuals with biallelic LoF variants (ID2 and ID9), an asymptomatic carrier (mother of ID2), and three controls (Fig. 3). As expected, unsupervised clustering and MDS analyses highlighted a major contribution of cell lineage on the observed grouping associated with the methylation status of the selected probes. However, both analyses were able to separate the affected individuals from controls within each lineage. Notably, the SVM algorithm properly classified the two affected individuals, and the four healthy controls with high confidence (SVM scores >0.9 and <0.1, respectively) (Fig. 3).

Genome-wide DNA methylation functional annotation analysis

To investigate the functional effect of biallelic *ZNF142* LoF variants on the genome-wide DNAm pattern in blood cells, both a site-based and a region-based approach were used. A total of 1407 DMPs (FDR < 0.05) were found when comparing the genome-wide DNAm patterns of the 18 individuals with biallelic *ZNF142* LoF variants and 288 healthy controls. The most significant DMPs included positions located in the promoter regions of the *GTPBP3/ANO8* (Fig. 4, top panel), *SCN2B* (Fig. 4, bottom panel), *SLC39A11*, *PTGES2*, and *OTUB2* genes (the 200 most significant DMPs are listed in Table S6; the 25 most significant DMPs are visualized in Fig. S6).

When applying a region-based approach using *DMRcate*, only 25 DMRs were found (Table S7). Of these, 13 were hypermethylated, while 12 were hypomethylated. The DMRs were predominantly located in the promoter regions or gene bodies, with a large degree of overlap in the results between the DMP and DMR analysis. Gene set enrichment analysis using the DMRs yielded no significant results for gene ontologies or pathways (FDR < 0.05). The most significant DMRs were located in the promoter regions of *GTPBP3/ANO8* (Fig. 4, top panel), *SLC39A11*, and *OTUB2*.

Comparison of the DNAm patterns of PB and FBs revealed similar patterns of beta-value change between individuals with biallelic *ZNF142* LoF variants and controls in the two tissues, when the most significant DMPs from the PB analysis was considered (Fig. 5). Specifically, an R^2 equal to 0.61 resulted when the 50 most significant probes were considered (44 probes present in the merged dataset), which increased to 0.71 when the 25 most significant probes were analyzed (23 probes present in the merged dataset) (Fig. 5). Ten probes showed a mean beta-value difference > 0.15 between individuals with biallelic *ZNF142* LoF

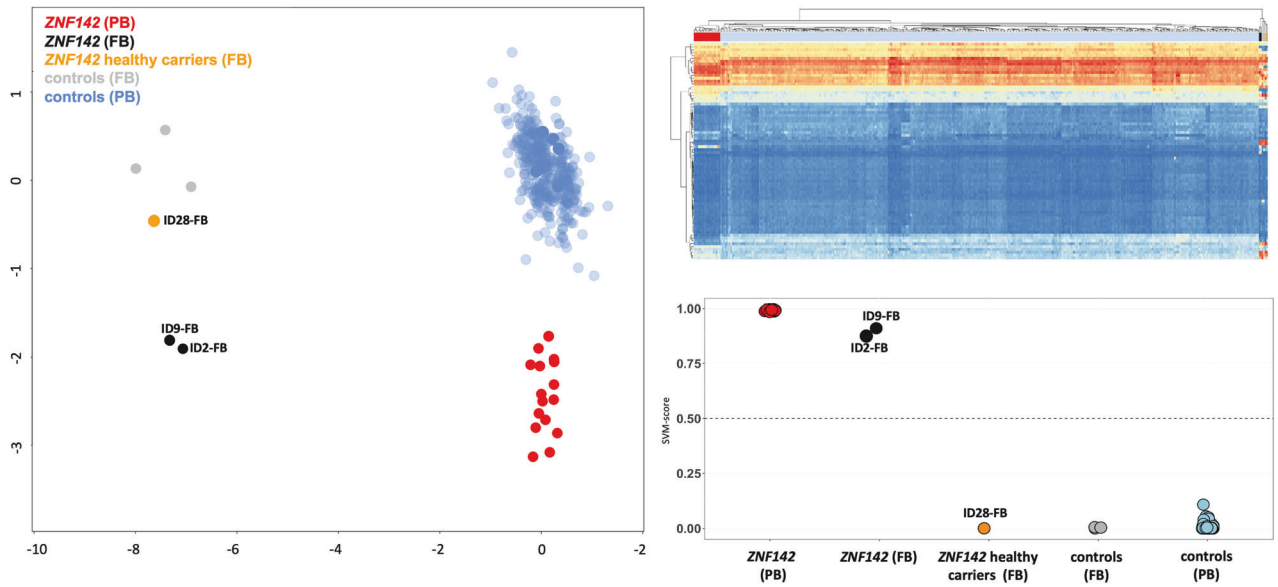

Fig. 3 The PB-derived DNAm signature successfully classifies DNA samples obtained from primary cultured fibroblasts of individuals with ZNF142 LoF and controls. The multidimensional scaling (MDS) plot shows the variance in DNAm between samples obtained from primary fibroblasts (FB) and peripheral blood (PB) (left panel). In the second dimension (Y-axis), a clear separation between individuals with biallelic *ZNF142* LoF variants (PB red dots, FB black dots) and controls (PB, blue dots; FB, gray dots) is observed. A FB sample from a heterozygous carrier of a *ZNF142* LoF variant (orange) clusters with the FB controls. Similarly, when considering the DNA samples obtained from FB, unsupervised hierarchical clustering separates individuals carrying biallelic *ZNF142* LoF variants from healthy individuals, including the tested sample with a heterozygous inactivating *ZNF142* variant (right top panel). The prediction scores from the machine learning classifier trained to recognize the PB DNAm signature of biallelic *ZNF142* LoF variants properly classifies the FB samples (right bottom panel), with FB-derived DNA samples from affected individuals receiving a prediction score of >0.9, and FB-derived DNA samples from the healthy carrier and other controls scored close to 0.

variants and controls in both PB and FB tissue (Table S8). These probes were located in or near *GTPBP3/ANO8, SLC39A11, ZNF215, CLIP2, RFC2, NEK3*, and *PTGES2*.

Different genome-wide studies have recently characterized the binding sites of many KRAB-ZFPs and defined their genomic targets as strongly biased toward TEs, with most of them displaying preferential enrichment at sequences present in one or several TE subtypes [43, 44]. To explore the possibility that the identified DMRs were enriched for any TEs, we carried out a genomic enrichment analysis, considering regions associated to different families of TEs, as short interspersed nuclear elements (SINE), long interspersed nuclear elements (LINE), long terminal repeat elements (LTR), and DNA repeat elements, as reported in RepeatMasker database. These analyses highlighted a significant overlap for a specific DNA repeat element family, hAT (GIGGLE score = 26.47; odds ratio = 41.53, Fisher's exact test = 1.19×10^{-5}), identifying this TE family as a putative regulatory target of ZNF142.

DISCUSSION

Biallelic LoF variants of *ZNF142* cause a clinically variable NDD without pathognomonic features, hampering genetic diagnosis, particularly in presence of VUS. In this study, we used PB-derived DNA samples of individuals carrying biallelic *ZNF142* LoF variants to resolve a genome-wide DNAm signature to be used as a tool to confirm or rule out the diagnosis of this disorder. The identified DNAm signature showed 100% sensitivity and specificity for biallelic LP/LP variants when applied to an internal control cohort including 277 healthy individuals and 123 subjects with various molecularly confirmed disorders. The episignature was successfully used for VUS reclassification, and was robust enough to properly classify the variants using DNA obtained from cultured FBs of two affected individuals.

So far, most variants associated with the *ZNF142*-related NDD involve splice sites, or cause premature termination of the coding sequence, pointing to ZNF142 LoF as the disease mechanism. Prior to this study, only five missense *ZNF142* changes (p.Arg581Cys, p.Ser763Cys, p.Cys1233Phe, p.Phe1295Leu, and Arg1500Trp) were reported in four unrelated affected individuals [1–3]. None of these variants has been functionally validated, and they are still classified as VUS according to the ACMG criteria. Here, we trained a ML classifier to reclassify the genotypes of two of these individuals/families (ID20 and ID21) together with six previously unreported individuals from three families (ID22, ID23-ID26, and ID27) with biallelic *ZNF142* variants which could not readily be classified as LP/P. When applying the ML classifier, ID20 and ID21 (p.Cys1233Phe/Arg1500Trp and p.Arg636*/p.Phe1295Leu, respectively) received a score indicating a partial match with the DNAm signature. The DNAm pattern for the selected probe set was compatible with a hypomorphic behavior of these missense variants. These substitutions are within the *C*-terminal ZnF motifs 15–31, and previous protein modeling studies carried out by our group predicted their damaging effect by affecting ZnF structure or binding to DNA [2]. Consistent with our findings, individuals ID20 and ID21 were reported to show a phenotype on the milder end of the clinical spectrum associated with ZNF142 LoF. The phenotype of ID20 comprised low average IQ (full scale IQ 78), age of walking of 18 months, lower limb hyper-reflexia and childhood apraxia of speech, but she did not have seizures or dysmorphism [1], while ID21 had normal cognitive development and the main symptoms included abnormal balance without clear ataxia, hypotonia, and some atypical seizures with normal EEG [2]. On the other hand, the group of three families ID22 (p.Gly1089Ser/p.Val780Ile), ID23-ID26 (p.Gly1055Arg/p.Val1553Met), and ID27 (p.Arg593His/p.Arg593His) did not match with the DNAm signature, making a diagnosis of *ZNF142*-related disorder unlikely. In line with these findings,

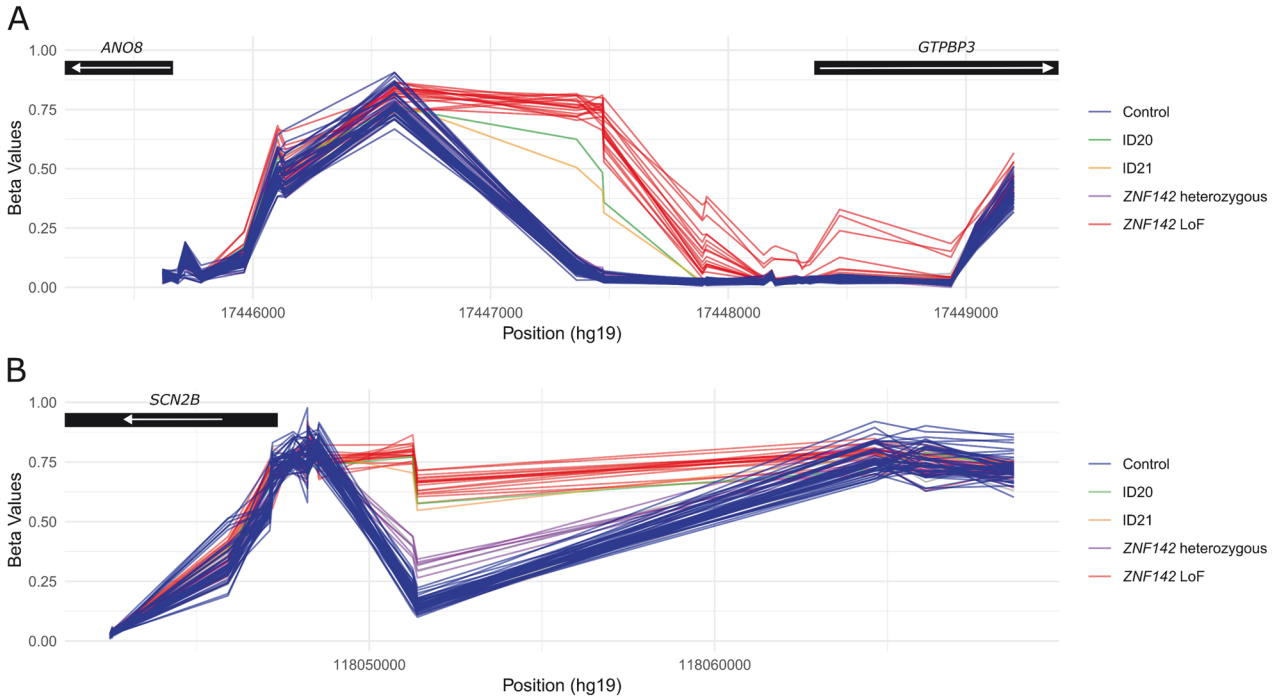

Fig. 4 Differences in the level of DNAm within the *GTPBP3*, *ANO8* and *SCN2B* loci between PB-derived DNA samples of affected individuals and controls. The panels show an increased methylation status of probes mapping to the promoter regions of *GTPBP3* and *ANO8* (**A**) and those at the promoter region of *SCN2B* (**B**) in DNA samples from affected individuals (red lines) compared to controls (blue lines). Individuals ID20 (green line) and ID21 (orange line) show intermediate methylation levels between affected individuals and controls, while heterozygous carriers (purple lines) have a similar methylation profile to controls.

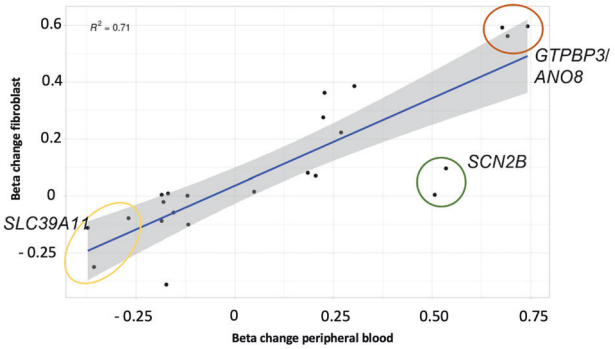

Fig. 5 Comparison of DNAm difference between individuals with biallelic *ZNF142* LoF variants and controls in different tissues. The dotplot shows the correlation between the average DNAm levels (beta change) in samples obtained from peripheral blood (PB) and primary fibroblasts (FB) for the top 25 differentially methylated probes.

subsequent segregation analysis documented that the two variants in ID22 were both maternally inherited, and clinical reassessment in the others affected individuals provided evidence of a clinical condition diverging from the spectrum caused by ZNF142 LoF. Except for the p.Arg593His variant, the substitutions that could be modeled did not predict any substantial structural consequence (*i.e.*, p.Val1553Met variant, see Fig. S5). Notably, while molecular dynamics simulations of p.Arg593His suggested that this substitution would affect the interaction of ZNF142 with the recognition site on the DNA molecule, it was classified with controls in both unsupervised and supervised DNAm analyses, indicating that the homozygous p.Arg593His substitution is not qualitatively equivalent to the inactivating or hypomorphic variants currently implicated in the ZNF142-related disorder. Further dedicated work is required to rule out a pathogenic effect of this variant and to investigate whether missense variants involving the *N*-terminal ZnF motifs contribute to disease pathogenesis.

The early establishment of altered genome-wide DNAm patterns during development makes possible the design and use of disease-specific probe sets that can be successfully applied to peripheral blood cells to confirm/rule out a clinical diagnosis [25]. However, the degree to which a blood cell-derived DNAm signature can be applied to other tissues/cell lineages is not an obvious assumption, as different tissues are expected to have unique disease-specific methylation patterns that do not necessarily overlap with those occurring in blood cells. Unexpectedly, comparison of the DNAm patterns characterizing PB and FBs revealed a significant degree of conservation among the most differentially methylated probes. Consistently, the PB-derived probe set successfully classified two individuals with biallelic pathogenic *ZNF142* variants as well as four healthy controls also when applied to FBs. While additional FB-derived DNA samples should be tested to confirm these findings, we predict that the identified episignature is stable to a large degree across different tissues, suggesting an underlying conserved regulatory mechanism shared by various cell lineages controlled by ZNF142 through its action on target genomic loci.

A second notable finding is that biallelic *ZNF142* LoF variants result in a dysregulation of DNAm levels with a large effect size at a small number of specific promoter regions, particularly those of *GTPBP3*, *SCN2B*, *SLC39A11*, *OTUB2*, and *SLC2A3*. A plausible explanation for this finding is that, like other KRAB-ZFPs, ZNF142 binds to longer DNA sequences compared to other transcription factors [45], likely resulting in an increased specificity. KRAB-ZFPs have previously been implicated in site-specific DNAm changes [14–16], and the present findings parallel to the multilocus imprinting disturbances previously attributed to pathogenic *ZFP57* and *ZNF445* variants [15, 46, 47]. A major difference is that the

reported DNAm changes in individuals with *ZNF142*-associated NDD do not occur within the imprinted regions. Furthermore, the differential methylation pattern related to ZNF142 LoF appears more specific when compared to what is observed for biallelic LoF *ZFP57* variants, which generally affect multiple imprinted loci [46]. Notably, both hypermethylated and hypomethylated DMRs are associated with ZNF142 LoF, which differs from recent findings on biallelic inactivating variants of *ZNF699*, where hypermethylation predominantly occurs [48].

While the DNAm signature associated with ZNF142 LoF correctly classified the healthy heterozygous individuals with controls, the two groups were distinguished by identifying a second set of DMPs, indicating a gene dosage effect on DNAm levels. Interestingly, these results also raise the possibility of DNAm signature fine-tuning to better characterize hypomorphic variants for diagnosing ZNF142-related disorders. Similar findings were recently obtained in DEGCAGS syndrome [48], a recessive syndromic NDD caused by LoF variants in *ZNF699*. Intermediate DNAm patterns have also been observed between affected hemizygous males and asymptomatic heterozygous females also for X-linked recessive disorders, such as those caused by LoF variants of *KDM5C* and *BRWD3* [20, 49], which suggests that a gene dosage effect on DNAm may represent a more general feature, even in absence of a clinical phenotype.

A recent study using a knock-in (KI) mouse model resulting in Znf142 LoF (*Znf142*^{Arg1508*}) provided evidence of a pattern of differentially expressed genes in the brain of homozygous KI mice [9]. Four of the identified differentially expressed genes, *Arl6ip5*, *Scn2b*, *Slc2a3*, and *Slc25a23*, were also found to have differentially methylated promoter regions in affected individuals with biallelic LoF *ZNF142* variants. Among these, *Scn2b* showed a 22-fold expression decrease in cerebellum and hypothalamus of KI mice. Consistently, two sites in the promoter/enhancer region of *SCN2B* showed the second largest differentially hypermethylated pattern in the present analyses. Only two probes in this region were available on the EPIC v.1 array, which likely explains why this locus was not identified as DMR. *SCN2B* codes for an isoform of the auxiliary β subunit of the voltage-sensitive sodium channel. The most significant methylation changes were in the promoter region of *GTPBP3* and *ANO8*, where large DNAm changes were observed in both PB and FB samples, and a methylation beta-value difference of 0.85 was observed at one probe in PB.

Functional annotation of the differentially methylated loci indicated a significant enrichment for the hAT family of TEs. KRAB-ZFPs were shown to act as major repressors of TEs, with underlying sequence-specificity attributed to unique combinations of ZnF motifs that target different retrotransposon families [50]. Of note, the various TE classes are differentially enriched among the KRAB-ZFPs targets. While LINEs, endogenous retroviruses, and SINE-VNTR-Alus are generally enriched as targets of KRAB-ZFPs, DNA TEs, including the hAT family, are the only class significantly underrepresented [50]. Our findings suggest that this specific TE family may be a pivotal target of ZNF142 to regulate neurodevelopmental processes [50].

In summary, we show that biallelic *ZNF142* LoF variants are associated with robust DNAm changes at a relatively limited number of loci, which are shared by multiple cell lineages. Our data provide an informative tool that can be applied for the clinical reclassification of *ZNF142* VUS, and document that hypomorphic variants explain, at least in part, the clinical variability characterizing the *ZNF142*-related disorder.

DATA AVAILABILITY

The clinical data of the study cohort and probes defining the DNA methylation signature associated with ZNF142 loss of function are provided in the supplemental data. The new variants reported in this work have been submitted to ClinVar (SCV006074640 to SCV006074664). The DNA methylation datasets generated and/or used in the study are not publicly available due to privacy/ethical/legal restrictions. Data are available from one of the corresponding authors (MT) upon request and permission of the individual participating subjects/legal guardians.

REFERENCES

1. Khan K, Zech M, Morgan AT, Amor DJ, Skorvanek M, Khan TN, et al. Recessive variants in ZNF142 cause a complex neurodevelopmental disorder with intellectual disability, speech impairment, seizures, and dystonia. Genet Med. 2019;21:2532–42.
2. Christensen MB, Levy AM, Mohammadi NA, Niceta M, Kaiyrzhanov R, Dentici ML, et al. Biallelic variants in ZNF142 lead to a syndromic neurodevelopmental disorder. Clin Genet. 2022;102:98–109.
3. Kamal N, Khamirani HJ, Mohammadi S, Dastgheib SA, Dianatpour M, Tabei SMB. ZNF142 mutation causes neurodevelopmental disorder with speech impairment and seizures: novel variants and literature review. Eur J Med Genet. 2022;65:104522.
4. Kameyama S, Mizuguchi T, Fukuda H, Moey LH, Keng WT, Okamoto N, et al. Biallelic null variants in ZNF142 cause global developmental delay with familial epilepsy and dysmorphic features. J Hum Genet. 2022;67:169–73.
5. Erro R, Sorrentino C, Russo M, Giordano C, Barone P. Focal head tremor and ZNF142-associated neurodevelopmental disorder. Mov Disord Clin Pr. 2023;10:1693–4.
6. Mir A, Song Y, Lee H, Montazer-Zohouri M, Reisi M, Tabatabaiefar MA. A deleterious frameshift insertion mutation in the ZNF142 gene leads to intellectual developmental disorder with impaired speech in three affected siblings: clinical features and literature review. Mol Genet Genom Med. 2023;11:e2261.
7. Al Masseri Z, Alqahtani M, Almoshawer E, Alkuraya FS. Vitamin D-binding protein deficiency: an underrecognized Mendelian disorder of vitamin D metabolism. Hum Genet. 2024;143:101–5.
8. Kaya D, Ceylan Köse C, Akcan MB, Silan F. A case report of a patient with neurodevelopmental disorder with impaired speech and hyperkinetic movements: a biallelic variant in the ZNF142 gene. Am J Med Genet A. 2024;194:e63636.
9. Proskorovski-Ohayon R, Eskin-Schwartz M, Shorer Z, Kadir R, Halperin D, Drabkin M, et al. ZNF142 mutation causes sex-dependent neurologic disorder. J Med Genet. 2024;61:566–77.
10. Bonchuk AN, Georgiev PG. C2H2 proteins: evolutionary aspects of domain architecture and diversification. Bioessays. 2024;46:e2400052.
11. Huntley S, Baggott DM, Hamilton AT, Tran-Gyamfi M, Yang S, Kim J, et al. A comprehensive catalog of human KRAB-associated zinc finger genes: insights into the evolutionary history of a large family of transcriptional repressors. Genome Res. 2006;16:669–77.
12. Al-Naama N, Mackeh R, Kino T. C2H2-type zinc finger proteins in brain development, neurodevelopmental, and other neuropsychiatric disorders: systematic literature-based analysis. Front Neurol. 2020;11:32.
13. Urrutia R. KRAB-containing zinc-finger repressor proteins. Genome Biol. 2003;4:231.
14. Oleksiewicz U, Gładych M, Raman AT, Heyn H, Mereu E, Chlebanowska P, et al. TRIM28 and interacting KRAB-ZNFs control self-renewal of human pluripotent stem cells through epigenetic repression of pro-differentiation genes. Stem Cell Rep. 2017;9:2065–80.
15. Monteagudo-Sánchez A, Hernandez Mora JR, Simon C, Burton A, Tenorio J, Lapunzina P, et al. The role of ZFP57 and additional KRAB-zinc finger proteins in the maintenance of human imprinted methylation and multi-locus imprinting disturbances. Nucleic Acids Res. 2020;48:11394–407.
16. Fukuda K, Makino Y, Kaneko S, Shimura C, Okada Y, Ichiyanagi K, et al. Potential role of KRAB-ZFP binding and transcriptional states on DNA methylation of retroelements in human male germ cells. Elife. 2022;11:e76822.
17. Ecco G, Cassano M, Kauzlaric A, Duc J, Coluccio A, Offner S, et al. Transposable elements and their KRAB-ZFP controllers regulate gene expression in adult tissues. Dev Cell. 2016;36:611–23.
18. Pontis J, Planet E, Offner S, Turelli P, Duc J, Coudray A, et al. Hominoid-specific transposable elements and KZFPs facilitate human embryonic genome activation and control transcription in naive human ESCs. Cell Stem Cell. 2019;24:724–35.e5.
19. Fahrner JA, Bjornsson HT. Mendelian disorders of the epigenetic machinery: tipping the balance of chromatin states. Annu Rev Genom Hum Genet. 2014;15:269–93.
20. Aref-Eshghi E, Kerkhof J, Pedro VP, France G, Barat-Houari M, et al. Evaluation of DNA methylation episignatures for diagnosis and phenotype correlations in 42 Mendelian neurodevelopmental disorders. Am J Hum Genet. 2020;106:356–70.
21. Aref-Eshghi E, Bend EG, Colaiacovo S, Caudle M, Chakrabarti R, Napier M, et al. Diagnostic utility of genome-wide DNA methylation testing in genetically unsolved individuals with suspected hereditary conditions. Am J Hum Genet. 2019;104:685–700.

22. Chater-Diehl E, Goodman SJ, Cytrynbaum C, Turinsky AL, Choufani S, Weksberg R. Anatomy of DNA methylation signatures: Emerging insights and applications. Am J Hum Genet. 2021;108:1359–66.
23. Levy MA, McConkey H, Kerkhof J, Barat-Houari M, Bargiacchi S, Biamino E, et al. Novel diagnostic DNA methylation episignatures expand and refine the epigenetic landscapes of Mendelian disorders. Hum Genet Genome Adv. 2021;2:100075.
24. Schenkel LC, Aref-Eshghi E, Rooney K, Kerkhof J, Levy MA, McConkey H, et al. DNA methylation epi-signature is associated with two molecularly and phenotypically distinct clinical subtypes of Phelan-McDermid syndrome. Clin Epigenetics. 2021;13:2.
25. Kerkhof J, Rastin C, Levy MA, Relator R, McConkey H, Demain L, et al. Diagnostic utility and reporting recommendations for clinical DNA methylation episignature testing in genetically undiagnosed rare diseases. Genet Med. 2024;101075.
26. Niceta M, Ciolfi A, Ferilli M, Pedace L, Cappelletti C, Nardini C, et al. DNA methylation profiling in Kabuki syndrome: reclassification of germline KMT2D VUS and sensitivity in validating postzygotic mosaicism. Eur J Hum Genet. 2024;32:819–26.
27. Richards S, Aziz N, Bale S, Bick D, Das S, Gastier-Foster J, et al. Standards and guidelines for the interpretation of sequence variants: a joint consensus recommendation of the American College of Medical Genetics and Genomics and the Association for Molecular Pathology. Genet Med. 2015;17:405–24.
28. Ciolfi A, Foroutan A, Capuano A, Pedace L, Travaglini L, Pizzi S, et al. Childhood-onset dystonia-causing KMT2B variants result in a distinctive genomic hypermethylation profile. Clin Epigenetics. 2021;13:157.
29. Pagliara D, Ciolfi A, Pedace L, Haghshenas S, Ferilli M, Levy MA, et al. Identification of a robust DNA methylation signature for Fanconi anemia. Am J Hum Genet. 2023;110:1938–49.
30. Chawla NV, Bowyer KW, Hall LO, Kegelmeyer WP. SMOTE: synthetic minority oversampling technique. J Artif Intell Res. 2002;16:321–57.
31. Meyer D, Dimitriadou E, Hornik K, et al. E1071: misc functions of the Department of Statistics (E1071). TU Wien R Package Vers. 2017;1:6–8.
32. Wickham H. ggplot2: elegant graphics for data analysis. J R Stat Soc A. 2011;174:245–6.
33. Peters TJ, Buckley MJ, Statham AL, Pidsley R, Samaras K, Lord RV, et al. De novo identification of differentially methylated regions in the human genome. Epigenetics Chromat. 2015;8:6.
34. Maksimovic J, Oshlack A, Phipson B. Gene set enrichment analysis for genome-wide DNA methylation data. Genome Biol. 2021;22:173.
35. Layer RM, Pedersen BS, DiSera T, Marth GT, Gertz J, Quinlan AR. GIGGLE: a search engine for large-scale integrated genome analysis. Nat Methods. 2018;15:123–6.
36. Hashimoto H, Wang D, Horton JR, Zhang X, Corces VG, Cheng X. Structural basis for the versatile and methylation-dependent binding of CTCF to DNA. Mol Cell. 2017;66:711–20.
37. Patel A, Yang P, Tinkham M, Pradhan M, Sun M-A, Wang Y, et al. DNA conformation induces adaptable binding by tandem zinc finger proteins. Cell. 2018;173:221–33.
38. Kelley LA, Mezulis S, Yates CM, Wass MN, Sternberg MJE. The Phyre2 web portal for protein modeling, prediction and analysis. Nat Protoc. 2015;10:845–58.
39. Waterhouse AM, Studer G, Robin X, Bienert S, Tauriello G, Schwede T. The structure assessment web server: for proteins, complexes and more. Nucleic Acids Res. 2024;52:W318–23.
40. Ros-Pardo D, Gómez-Puertas P, Marcos-Alcalde I. STAG2: computational analysis of missense variants involved in disease. Int J Mol Sci. 2024;25:1280.
41. Roe DR, Cheatham TE. PTRAJ and CPPTRAJ: software for processing and analysis of molecular dynamics trajectory data. J Chem Theory Comput. 2013;9:3084–95.
42. Humphrey W, Dalke A, Schulten K. VMD: visual molecular dynamics. J Mol Graph. 1996;14:33–8.
43. Imbeault H, Helleboid PY, Trono D. KRAB zinc-finger proteins. Nature. 2017;543:550–4.
44. de Tribolet-Hardy J, Thorball CW, Forey R, Planet E, Duc J, Coudray A, et al. Genetic features and genomic targets of human KRAB-zinc finger proteins. Genome Res. 2023;33:1409–23.
45. Fedotova AA, Bonchuk AN, Mogila VA, Georgiev PG. C2H2 zinc finger proteins: the largest but poorly explored family of higher eukaryotic transcription factors. Acta Nat. 2017;9:47–58.
46. Kagami M, Hara-Isono K, Matsubara K, Nakabayashi K, Narumi S, Fukami M, et al. ZNF445: a homozygous truncating variant in a patient with Temple syndrome and multilocus imprinting disturbance. Clin Epigenetics. 2021;13:181.
47. Bak M, Boonen SE, Dahl C, Hahnemann JMD, Mackay DJD, Tümer Z, et al. Genome-wide DNA methylation analysis of transient neonatal diabetes type 1 patients with mutations in ZFP57. BMC Med Genet. 2016;17:29.
48. Karimi K, Weis D, Aukrust I, Hsieh T-C, Horackova M, Paulsen J, et al. Epigenomic and phenotypic characterization of DEGCAGS syndrome. Eur J Hum Genet. 2024;32:1574–82.
49. Schenkel LC, Aref-Eshghi E, Skinner C, Ainsworth P, Lin H, Paré G, et al. Peripheral blood episignature of Claes-Jensen syndrome enables sensitive and specific identification of patients and healthy carriers with pathogenic mutations in KDM5C. Clin Epigenetics. 2018;10:21.
50. Kosuge M, Ito J, Hamada M. Landscape of evolutionary arms races between transposable elements and KRAB-ZFP family. Sci Rep. 2024;14:23358.

ACKNOWLEDGEMENTS

The authors thank the families who participated in this study. Several of the authors of this publication are members of the European Reference Network on Rare Congenital Malformations and Rare Intellectual Disability ERN-ITHACA (EU Framework Partnership Agreement ID: 3HP-HP-FPA ERN-01-2016/739516). The computational support of the "Centro de Computación Científica CCC-UAM" is gratefully recognized.

AUTHOR CONTRIBUTIONS

MH, AC and MF performed the DNA methylation analyses, prepared all figures and tables, and contributed to writing the manuscript. CC performed the DNA methylation microarray experiments and contribute to data analyses. PG-P, IM-A and DR-P performed the structural analyses. CAA, DJA, TSB, VB, OSB, BC, AC-G, MDW, MD-F, TBH, RAJ, RK, SK, BK, CK, IK, DL, RM, NM, AM, FM, KP, BAP, LR, KS, KVS, EV, JV, EW and MZ contributed to the clinical assessment of patients, DNA sample collection/processing and performed the genetic analyses. ZT and MT supervised all aspects of the work, and wrote the manuscript. All authors provided critical feedback on the manuscript.

FUNDING

This work was supported, in part, by Fonden for Neurologisk Forskning (R90-A4422, to MH), Italian Ministry of Research (FOE_2020, to MT), and Italian Ministry of Health (Current Research Funds and PNRR-MR1-2022-12376811, to MT; 5×1000_2023, to AC; Ricerca Corrente 2024, to MF).

COMPETING INTERESTS

The authors declare no competing interests.

ETHICAL APPROVAL

The study was approved by the local institutional review board (Ethical Committee, Ospedale Pediatrico Bambino Gesù, ref. 1702_OPBG_2018, 2072_OPBG_2020 and PNRR-MR1-2022-12376811). Clinical data, and DNA samples were collected, pseudonymized and stored in the context of routine diagnostic testing, following procedures in accordance with the ethical standards of the declaration of Helsinki protocols and subsequent versions after written signed informed consents from the participating individuals or parents/guardians were secured.

ADDITIONAL INFORMATION

Supplementary information The online version contains supplementary material available at https://doi.org/10.1038/s41431-025-01876-z.

Correspondence and requests for materials should be addressed to Zeynep Tümer or Marco Tartaglia.